Structural diversity and optoelectronic properties of chemical modification pentagonal quantum dots

Journal of Physics: Conference Series **2485** (2023) 012002 doi:10.1088/1742-6596/2485/1/012002

Structural diversity and optoelectronic properties of chemical modification pentagonal quantum dots

Pham Thi Bich Thao[1], Nguyen Thi My Hang[1], Nguyen Hai Dang[2], Pham Vu Nhat[1], and Nguyen Thanh Tien[1,†]

[1]College of Natural Sciences, Can Tho University, 3-2 Road, Can Tho City, Vietnam
[2]College of Basic Sciences, Nam Can Tho University, Nguyen Van Cu Street, Can Tho City, Vietnam

E-mail: nttien@ctu.edu.vn

Abstract. A first-principle study of the structural diversity and optoelectronic properties of the small penta-graphene quantum dots (PGQDs) has been performed. The stability and optoelectronic properties of the PGQDs are investigated under the effect of chemical modifications. PGQDs are edge functionalized by non-metallic atoms (Si, P, O, F) such as identical edge termination (Si-PGQD, P-PGQD, O-PGQD, F-PGQD) and alternate edge termination (Si-O-PGQD, H-P-PGQD). Further, H-PGQDs are also doped and co-doped with B and P atoms. All studied structures are stable with strong electronic quantization and exhibit semiconducting or metallic properties depending on the termination, doping elements and their site. Absorption peaks in the visible region were not observed for hydrogen passivation PGQDs. However, some absorption peaks appear in this region for edge-passivated. In addition, there are dramatic changes in the electronic properties of B, P, BP-doped PGQDs to give peak shifts to the visible region from the ultraviolet region of the pure sample due to hybridization effects. The enhanced reactivity, controllable electronic properties of edge passivation, and doping make PGQDs ideal for new nanodevice applications.

1. Introduction

In past decades, fluorescent type of semiconductor nanoparticles - Quantum dots (QDs) have attracted lot of popularity among researchers' due to their unique opto-electronic properties and relevant applications [1, 2]. Specifically, QDs have applied in energy devices, catalysis, sensing, photodynamic and photothermal therapy, drug delivery, and bioimaging. Until now, QDs like carbon quantum dots, graphene quantum dots (GQDs) and zinc oxide quantum dots have extensively studied in theoretical and experimental works [3, 4]. Recently, various two-dimensional (2D) nanomaterials with novel pentagonal structures such as penta graphene (PG), penta-silicene, penta-CB_2, transition metal dichalcogenides [5, 6, 7, 8, 9] have been predicted. In addition, the structural stability of the 2D pentagonal $PdSe_2$ and PdPSe materials have been successfully analyzed [10, 11] to promote the development of penta materials. Among them, penta graphene - the latest allotrope of carbon is expected to be one of the novel materials that can improve the size and properties of the device.

In previous work, the GQDs or PGQDs were made up of hexagonal or pentagonal rings [3, 12]. This also caused the appearance of free electrons at the edge atoms, so passivation is one of the popular ways to enhance stability for quantum dot structures. For PGQDs (or GQDs),

it is common to use hydrogen atom for edge passivation [13, 14]. However, to investigate novel electronic and optical properties, it can be used different atoms to passivate penta-graphene nanoribbon (or graphene nanoribbon) and GQDs [15, 16, 17, 18]. Moreover, doping is also one of the conventional methods to learn about unique optical properties [19, 20]. In addition, the thermodynamic stability of our investigated PGQDs also exhibit an increase with an increase in the size of the quantum dots [12, 21]. In particular, the search for absorbent materials in the visible light region to expand applications from solar energy is being studied extensively. Therefore, in this study, we choose group-III, -IV, -V, -VI elements (B, Si, P, O) with radii similar to carbon to study of the effect of passivation and doping on the electronic and optical properties using density functional theory (DFT). The lateral sizes of the GQDs have been determined to be from 10 Å to 200 Å in diameter [21, 22].

In this study, we consider PGQDs with small size and zigzag border morphology with 36 carbon atoms (ZZ-36-PGQDs), which have the stable ability [12, 21]. Our calculation reveals that these quantum dots are thermally stable in vacuum and the properties of PGQDs depend strongly on the type of functional atom, and the type of doping atom. The cause of those effect can be traced back to the variety of atomic orbital hybridizations. These results highlight the use of group-III, -IV, -V, -VI elements to develop PGQDs in optoelectronic devices.

2. Methodology

From the 2D PG structure, ZZ-36-PGQDs are generated. Next, this structure is passivated by Silicon (Si), Phosphorus (P), Oxygen (O) and Flourine (F), respectively. In addition, ZZ-36-PGQDs passivated by alternate edge termination (combination of two atoms) are also established. Due to its stability and high symmetry [12], H-36 (ZZ-36-PGQDs were passivated by the hydrogen atoms) is further doped or co-doped by Boron (B) and Phosphorous (P). The structures were optimized by CASTEP code [23] within the DFT method using the generalized gradient approximation (GGA) for Perdew Burker Ernzerhof (PBE) exchange-correlation functional [24] with the condition: k-point 1x1x1 and a cutoff energy 500-1000 eV. To avoid interaction between periodic images of the structure, a 15 Å vacuum region was applied for Ox, Oy, and Oz-directions of the studied samples. The convergence precision of energy for the maximum energy change, the maximum residual force on each atom, the maximum stress, and the maximum displacement were 10^{-6} eV/atom, 0.01 eV/Å, 0.1 GPa, and 0.001 Å, respectively.

The electronic and optical properties of the optimized structures were performed in the Atomistix ToolKit (ATK) software package (version 2018) by DFT computing with the GGA-PBE function and a double-zeta polarized basis sets [25, 26]. In all calculations, one k-point (G point), mesh cutoff energy of 1000 eV were used, and the Fermi level ($E_F = 0$) was set at zero.

The optical properties of the investigated structures will be determined by the complex dielectric functions [27]

$$\varepsilon(\omega) = \varepsilon_1(\omega) + \mathbf{i}\varepsilon_2(\omega), \tag{1}$$

the real and imaginary parts of the dielectric function are ε_1 and ε_2, respectively. The angular frequency of the incident photon is ω. The susceptibility $\chi(\omega)$ is calculated by the Kubo–Greenwood formula [28],

$$\chi_{ij}(\omega) = -\frac{e^2\hbar^4}{m_e^2\varepsilon_0 V\omega^2}\sum_{mn}\frac{f(E_m) - f(E_n)}{E_{nm} - \hbar\omega - i\hbar\Gamma} \times \pi_{nm}^{i}\pi_{mn}^{j}, \tag{2}$$

here, $\pi_{nm}^{i,j}$ means i, j - components of the dipole matrix element between n and m states, Γ is the broadening, V is the volume, $f(E_m/E_n)$ is the Fermi function and $E_m(E_n)$ corresponds to

eigenvalues of $m\,(n)$ state. The extinction coefficient κ will be calculated

$$\kappa = \sqrt{\frac{\sqrt{\varepsilon_1^2 + \varepsilon_2^2}}{2} - \frac{\varepsilon_1}{2}}. \tag{3}$$

The optical absorption coefficient of the materials will be perfomed

$$\alpha = \frac{2\omega\kappa}{c}, \tag{4}$$

where, c is the velocity of light in vacuum.

3. Results and discussion

3.1. Effect of passivation on electronic and optical properties of PGQD

ZZ-36-PGQDs are passivated by Si, P, O, F atom after optimization, denoted Si-36, P-36, O-36 and F-36, are presented in Fig.1. The stability of the structures are determined through the binding energy E_B

$$E_B = \frac{(E_{total} - n_C E_C - n_X E_X)}{n_C + n_X}, \tag{5}$$

where, the total energy for one unit cell and the isolated energy for one C and X atom are E_{total}, E_C and E_X. The number of C and X atoms are n_C and n_X.

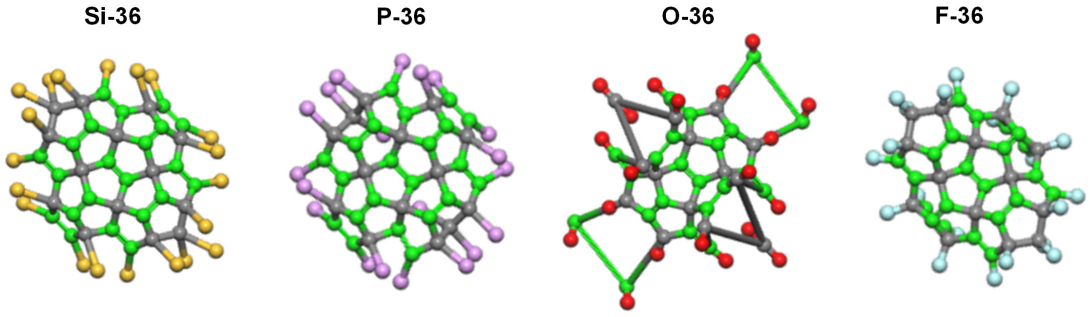

Figure 1. Configurations of PGQDs are passivated by Si, P, O, F atom after optimization. Gray and green balls represent for sp^3 hybridized carbon atom and sp^2 hybridized carbon atom, respectively. Yellow, violet, red and sky blue balls represent for Si, P, O, F atom, respectively.

The binding energy values of Si-36, P-36, O-36 and F-36 are -5.34 eV, -5.17 eV, -5.96 eV and -5.24 eV, respectively, indicating that these structures are thermally stable. Among the selected edge-functionalized atoms, oxygen atom stands out as an excellent candidate to stabilize these PGQDs due to the largest absolute binding energy. The average bond lengths of Si-36, P-36, O-36, F-36 structures before and after optimization are shown in Table 1. Atomic radii of Si and P are larger than atomic radii of O and F. In addition, the bond length is also affected by the hybridization form. As a result, the significant change in average bond length between sp^3 hybridized carbon atom and Si (P) atoms ($sp^3 - edge$) is observed after optimization. For F-36, average bond length between sp^3 hybridized carbon atom and F atoms ($sp^3 - edge$) rises about 17%. In contrast, the average bond lengths between sp^3 hybridized carbon atom and O

Table 1. The average bond length of Si-36, P-36, O-36 and F-36 (Å).

Before optimization				
	Si-36	P-36	O-36	F-36
$sp^2 - sp^2$	1.631	1.631	1.631	1.631
$sp^2 - sp^3$	1.536	1.536	1.536	1.536
$sp^3 - sp^3$	1.536	1.536	1.536	1.536
$sp^2 - egde$	1.140	1.140	1.140	1.140
$sp^3 - egde$	1.140	1.140	1.140	1.140
After optimization				
	Si-36	P-36	O-36	F-36
$sp^2 - sp^2$	1.391	1.426	1.914	1.346
$sp^2 - sp^3$	1.511	1.533	2.072	1.525
$sp^3 - sp^3$	1.526	1.568	x	1.594
$sp^2 - egde$	1.098	1.828	1.141	1.331
$sp^3 - egde$	2.095	1.947	1.181	1.383

atoms exhibits a little difference. However, the effect of O atom on the $sp^2 - sp^2$, $sp^2 - sp^3$ and $sp^3 - sp^3$ average bond lengths is significant. The structural change often strongly affects the properties of the material, so the optical and electronic properties of these PGQDs will be examined in detail in the next section.

From Figure 2, it can be seen, the change in band gap strongly depends on passivation atoms. P-36 structure has metallic properties, while other structures (Si-36, O-36, F-36) have semiconducting properties with band gap from 0.7 eV to 3.3 eV. This is similar to the obtained results for P doping or P passivation in a penta-graphene sheet and penta-graphene nanoribbons [14, 15] due to the P atom belonging to the VA group with five electrons in the outer most orbit. Similar to graphene, the difference of the subband shift in the other samples (Si-36, O-36, F-36) can be elucidated by edge orbital hybridization and charge transfer between PGQDs and edge atoms [29]. This result is further clarified from density of state (DOS) and partial density of state (PDOS) depicted in Figure 3. Specifically, for Si-36 and O-36, a significant contribution of Si, P, O atoms is observed around the Fermi level, leading to a dramatic reduction in the band gap compared with H-36. Meanwhile, the band gap of F-36 and H-36 are not much different because the contribution of F atom around the Fermi level compared with that of H atom in H-36 has not changed significantly.

The absorption spectra of Si-36, O-36, P-36 and F-36 are shown in Figure 3. In general, the anisotropy of the absorption spectrum is acquired in all of the above structures and the absorption peaks of the studied structures correspond to wavelengths in the visible or near-infrared region. Specifically, Si-36 structure exhibits the absorption peak in Oy direction at 1500 nm and in Ox and Oz direction in the wavelength range from 800 nm to 900 nm. Meanwhile, P-36, the spectral peak with the highest intensity corresponding to 1000 nm is observed in Oy direction. In this direction, there are also some additional spectral peaks at wavelengths corresponding to the visible or near-infrared regions (640 nm, 760 nm and 1680 nm). For O-36, the spectral peaks with the greatest intensity in all three directions stay in the visible light region with wavelengths of 700 nm, 450 nm and 435 nm in Ox, Oy and Oz direction, respectively. The obtained spectral peaks of F-36 are shifted to the higher energy region compared to those of

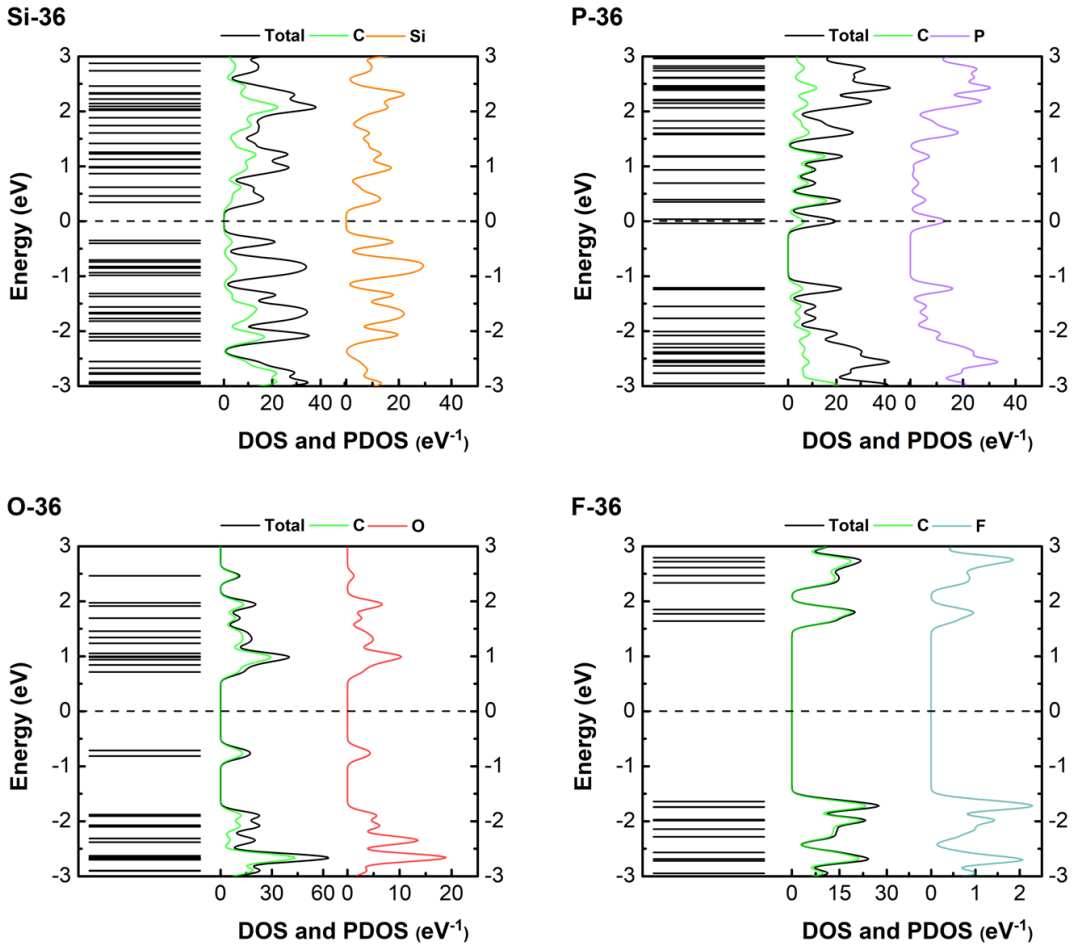

Figure 2. Band structure, density of state (DOS) and partial density of state (PDOS): a) Si-36, b) P-36, c) O-36 and d) F-36.

H-36, but these peaks are still in the ultraviolet region.

The above results show a close relationship between the electronic and optical properties of PGQDs. Obviously, the similarity of the absorption spectrum of H-36 and F-36 is obtained due to a little change of their band gap. In the structure with P edge atom, the band gap is more narrow and some spectral peaks appear in the red light region or in the vicinity. This is similar to a number of studies performed [29, 30]. For the O-36 structure with the band gap of 1.428 eV, the semiconducting characteristics are most clearly demonstrated. From the band structure, it can be observed that, the highest subband is about -0.7 eV to -0.8 eV and the next is about -2 eV in the valence band. The two spectral peaks are observed on Oy and Oz corresponding to the transition from these two energy levels to the lowest subband of the conduction band.

We also make edge changes of Si-36 and H-36 to form alternate edge termination structures. For Si-36 structure, four Si atoms were replaced by four O atoms as shown in Figure 3.9 to create the Si-O-36 structure. At the same time, six Si atoms were replaced by six O atoms (Fig.9) to create the structure Si-O-36-1. Similarly, for H-36 structure, eight or twelve atoms were replaced by eight or twelve P atoms to give H-P-36 and H-P-36-1 structures. Conditions to optimize and investigate electronic or optical properties are performed as in previous paragraph.

The stability of the structures is determined through the binding energy E_B (Eq. 5). The

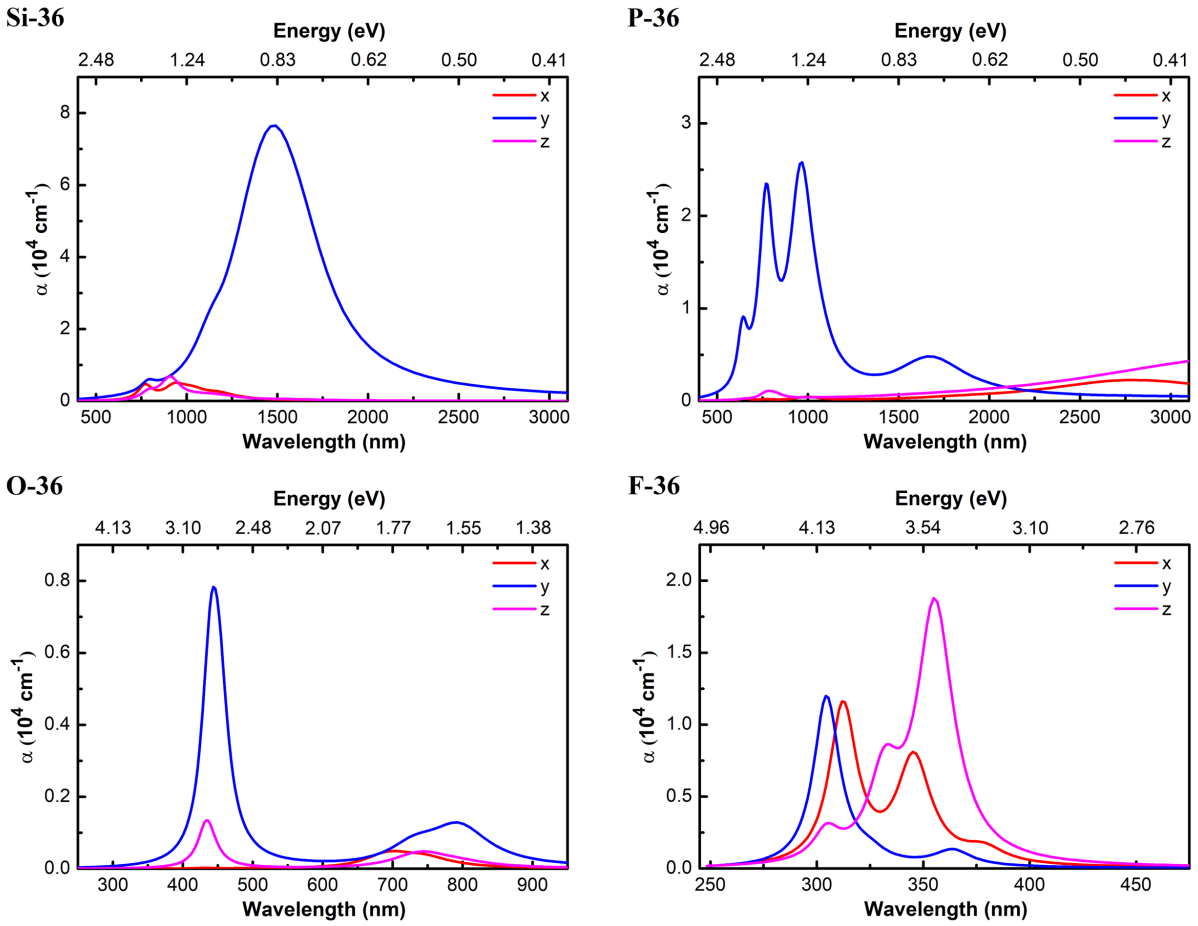

Figure 3. Optical absorption spectrum of the structures: Si-36, P-36, O-36 and F-36.

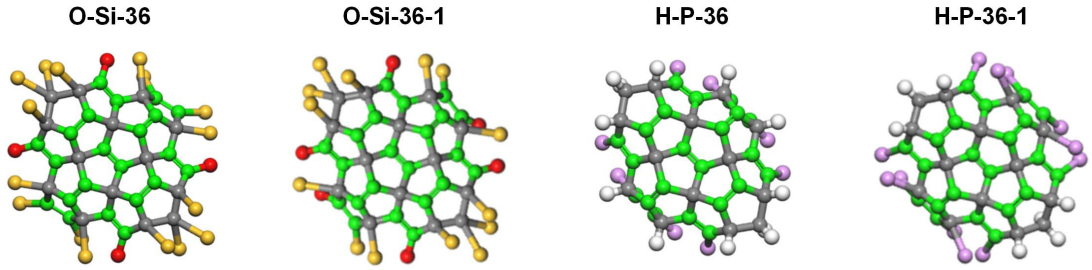

Figure 4. Configurations of O-Si-36, O-Si-36-1, H-P-36 and H-P-36-1 after optimization. Gray and green balls represent for sp^3 hybridized carbon atom and sp^2 hybridized carbon atom, respectively. Yellow, violet, red and white balls represent for Si, P, O, H atom, respectively.

numerical results show that the binding energy values of Si-O-36, Si-O-36-1, H-P-36 and H-P-36-1 are -5.64 eV, -5.83 eV, - 5.28 eV and -5.22 eV. In the above order, the Si-O-36-1 structure

has the lowest binding energy and the H-P-36-1 structure has the highest binding energy. These structures are thermally stable and the Si-O-36-1 structure is the most stable.

The average bond length difference was recorded between the sp^3, sp^2 hybridized carbon and the edge atoms (H, Si, O and P). For the Si-O-36 and Si-O-36-1 structures, the average bond length between the carbon atoms and sp^2-edge hybridization (sp^2-O) is smaller than the average bond length of the carbon atoms. The carbon atom has sp^3-edge hybridization (sp^3-Si) because the atomic radius of O is smaller than the atomic radius of Si. In addition, at the passivation site by two Si atoms, the average sp^3-Si bond length is the highest. For the H-P-36 and H-P-36-1 structures, the average bond lengths of sp^2-H, sp^3-H are homologous. A significant difference was obtained in the penta ring passivated by two P atoms (H-P-36) and the penta ring passivated by four P atoms (H-P-36-1). The interaction of the free electrons of the P atom in the H-P-36-1 structure is stronger and more obvious. As a result, the C-P bond length in this structure is larger than that of the H-P-36 structure. The obtained results are predicted to greatly affect the electronic and optical properties of PGQDs with alternate edge termination.

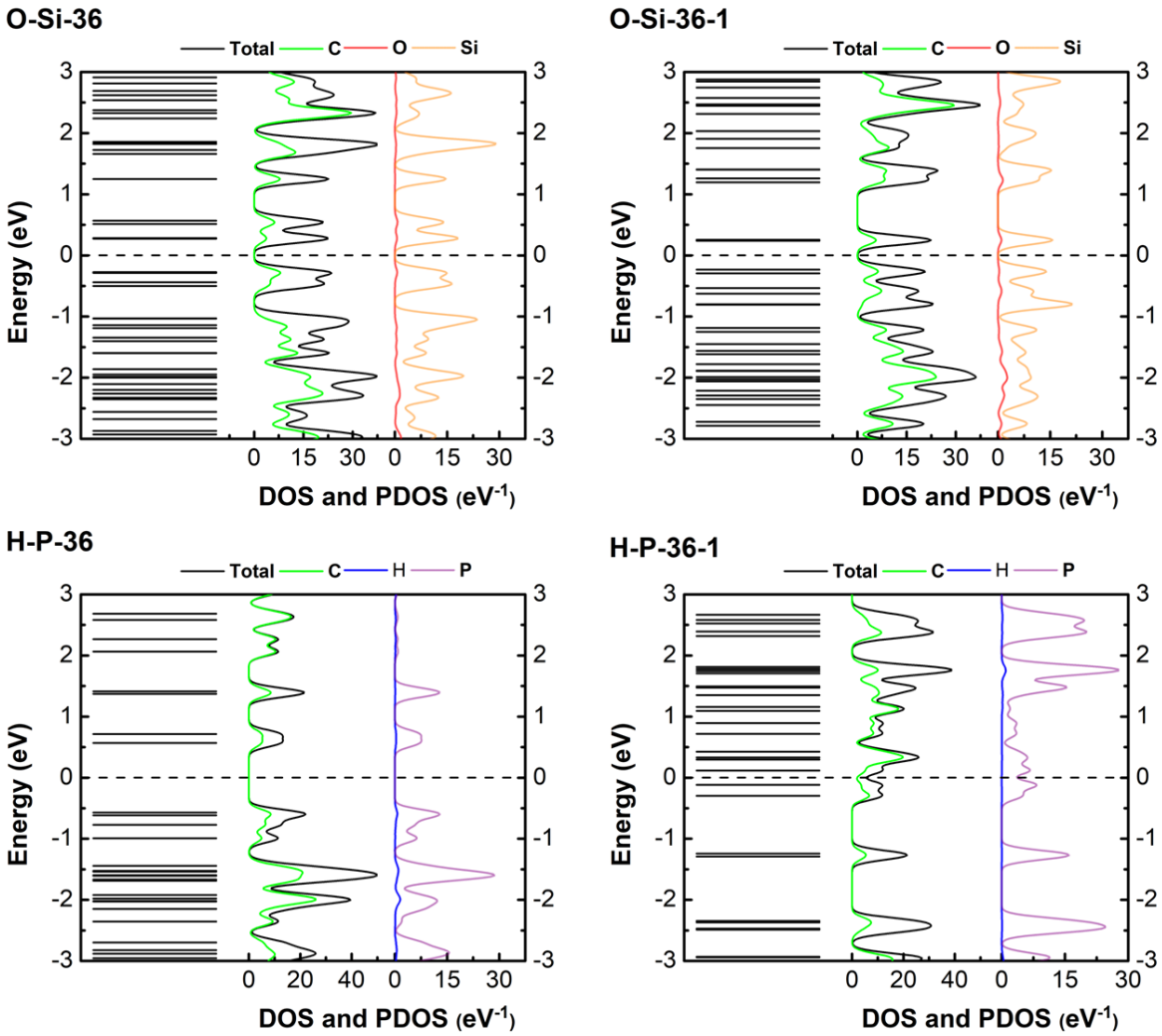

Figure 5. Band structure, density of state (DOS) and partial density of state (PDOS): Si-36, P-36, O-36 and F-36.

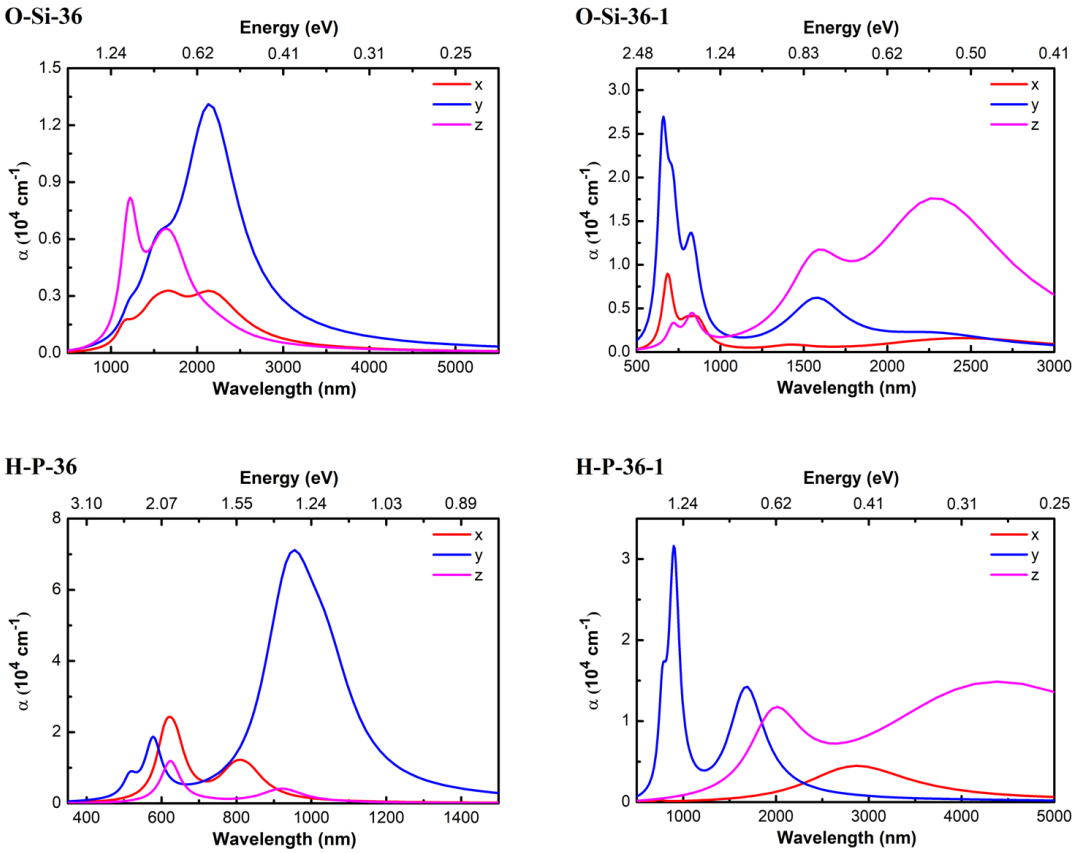

Figure 6. Optical absorption spectrum of the structures: Si-36, P-36, O-36 and F-36.

Figure 5 showed the band gap of Si-O-36 and Si-O-36-1 has changed compared to that of Si-36 structure. Specifically, the band gap of the Si-O-36 structure decreases by 0.15 eV, while that of the Si-O-36-1 structure decreases by 0.222 eV. In addition, the distribution of their subbands is different, which proves that the O atom has an important role to reduce the band gap. The band gap in the structures decreases as the number of O atoms increases. Similarly, the band gap of H-P-36 structure significantly reduces from 3.824 eV to 1.141 eV, while the H-P-36-1 structure has a band gap of 0.235 eV. It can be seen that, increasing the number of P atoms in H-36, the electronic properties of the structure tend to shift towards metal. This result is further clarified from the graph of total density of states (DOS) and partial density of states (PDOS). The PDOS plot presents changes in the electronic properties of the studied structures by the contribution of C atom and edge atoms.

The absorption spectra of the Si-O-36, Si-O-36-1, H-P-36 and H-P-36-1 structures are shown in Figure 6. The anisotropy of the absorption spectrum is captured in all functionalized PGQD structures. Their absorption peaks correspond to wavelengths in the near-infrared region and the intensity of the absorption peaks in Oy-direction is superior to those in Ox and Oz-directions. Particularly, the Si-O-36-1 and H-P-36 structures appear absorption peaks in the visible light region. Specifically, the Si-O-ZZ-1 structure has the largest peak intensity in Oy-direction at wavelength 650 nm, which is three times higher than the peak intensity in Oy direction. H-P-36 has the strongest peak intensity in Oy-direction at wavelength 950 nm. In this direction, there is an extra spectral peak in the visible region corresponding to the wavelength 590 nm. On the other hand, the two spectral peaks in Oz, Oz-directions are also at a wavelength 620 nm.

Meanwhile, H-P-36-1 structure, the highest peak intensity at 800 nm is observed on Oy-direction. In this direction, there is also an additional optical absorption peak in the near-infrared region.

3.2. Effect of doping on electronic and optical properties of PGQD

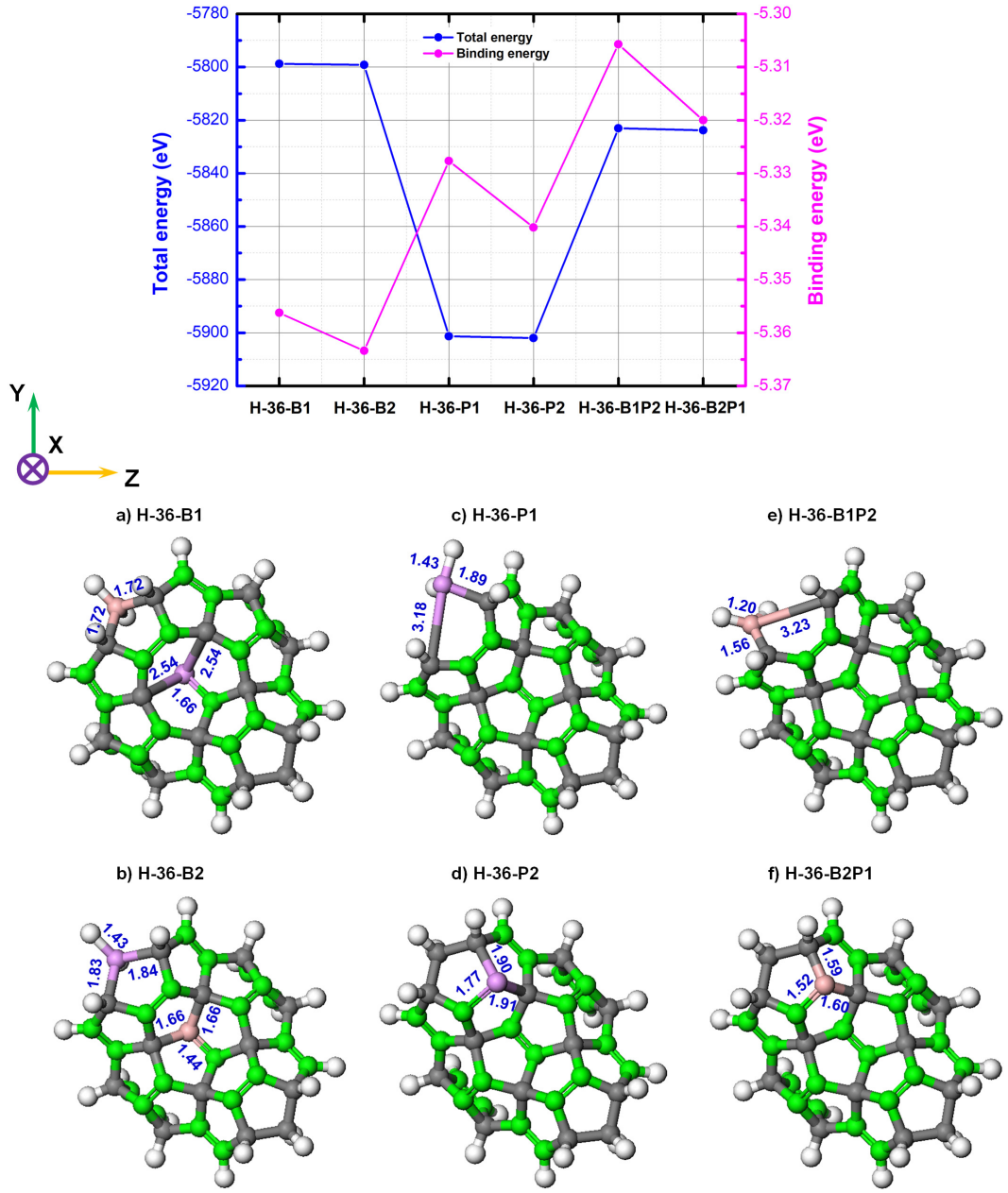

Figure 7. Total and binding energy graph of PGQDs doping B, P or BP. Optimized structures of six investigated PGQDs doping. The pink and violet ball represent boron and phosphorus atom.

In our previous results, H-36 presents the most stability due to the lowest formation energy [12]. However, the absorption peaks stay in the ultraviolet region because of a quite large band gap. The novel electronic and optical properties of this structure was predicted to yield many

interesting points by doping boron (B) and phosphorous (P) at sp^3 and sp^2 hybridized carbon atom, respectively (H-36-B1, H- 36-B2, H-36-P1 and H-36-P2) or co-doped with boron and phosphorous at the two characteristic carbon sites of PGQD (H-36-B1P2 and H-36-B2P1).

The total energy and the binding energy of six doped PGQDs are presented in Fig.7. For single-doped PGQD, the doped configuration at sp^2 hybridized carbon atom exhibits more stable for both boron and phosphorous doping of H-36. In Fig.7a and 7c, the doped penta ring structure is significantly deformed, while the stable structure is observed in Figures 7b and 7d. The co-doping for H-36-B1P2 and H-36-B2P1 show more stable compared to single-doped by considering the binding energy and morphology optimization. In this case, H-36-B2P1 has a lower binding energy and a more stable penta ring. Meanwhile, the bond lengths around the P atom of H-36-B2P1 change dramatically and increase the buckling of the penta ring.

Next, we will consider the effect of impurities on the electronic properties of PGQD. Band structures (BS) for six mentioned structures are shown in Fig.8. For single-doped PGQDs (H-36-B1, H-36-B2, H-36-P1 and H-36-P2) appear a subband coincides with the Fermi level.

This result shows that there is a transition from semiconductor to metal compared with pristine structure (H-36). The change is homologous to the B or N doped penta nanoribbon structure. In contrast, B and P co-doped PGQDs (H-36-B1P2 and H-36-B2P1) exhibit semiconducting properties. Specifically, band gaps are 1.50 and 1.14 eV, respectively. The partial density of states (PDOS) in Fig.8 and electron localization function (ELF) in Fig.9 can further clarify the influence of boron and phosphorous atoms on the electronic properties of PGQDs. For H-36-B1, H-36-B2, H-36-P1 and H-36-P2, the doping atom has created a state at the Fermi level that causes the corresponding subband in the band structure. On the other hand, in co-doped PGQD, the states of the atoms are not found at the Fermi level. In addition, the phosphorous contribution is greater than that of the boron at subbands near the Fermi level. In Fig.9, we can also explore localized increases of electron around B and P atoms.

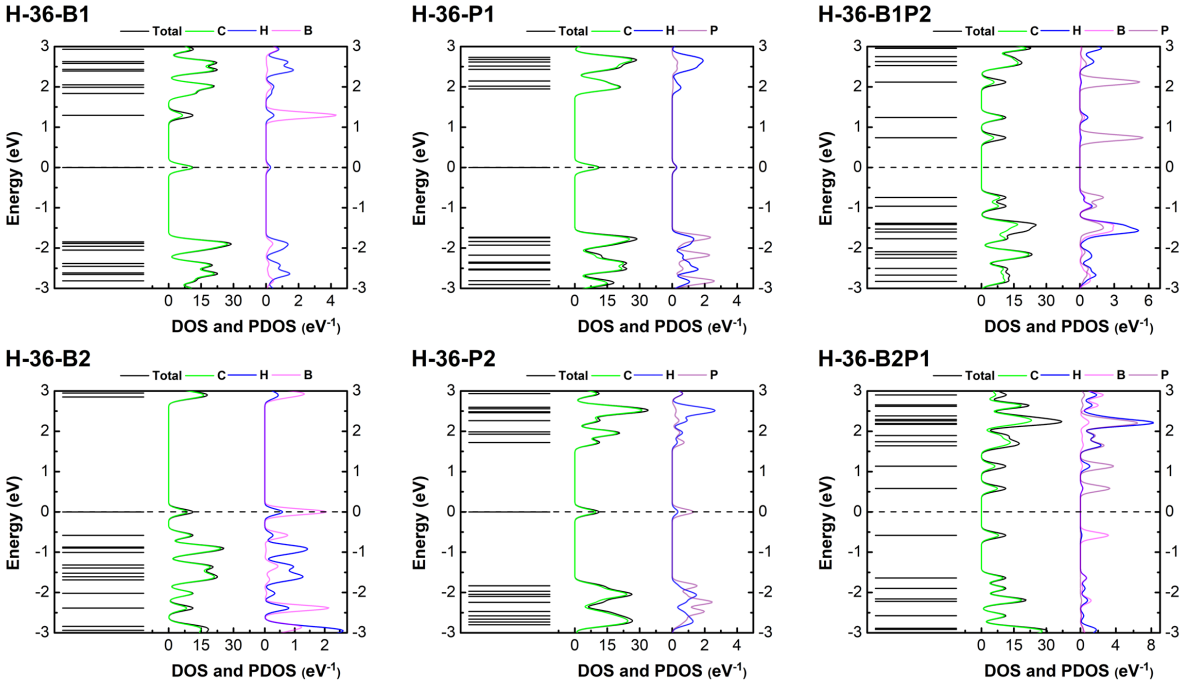

Figure 8. Band structure, density of state (DOS) and partial density of state (PDOS): H-36-B1, H-36-B2, H-36-P1, H-36-P2, H-36-B1P2 and H-36-B2P1.

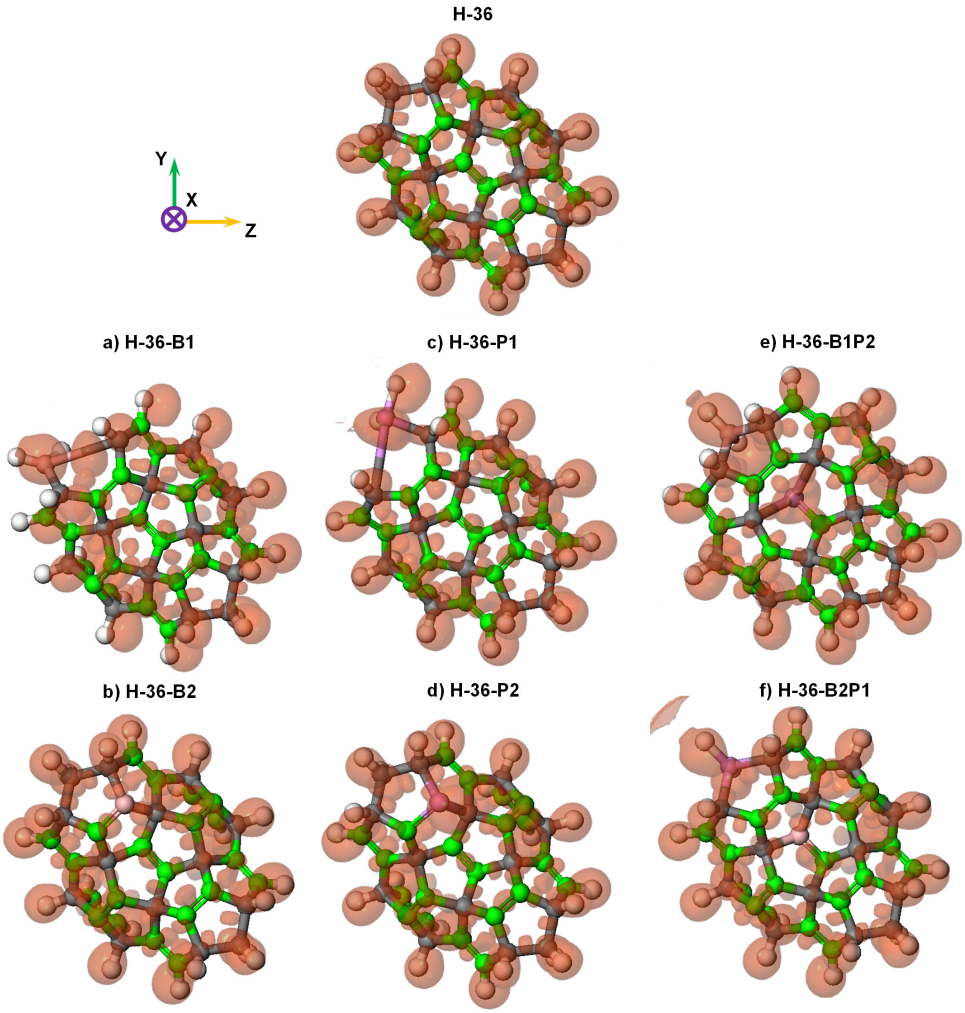

Figure 9. Electron localization function (ELF) map of doped PGQDs.

Explicitly, absorption peaks are observed in the ultraviolet and visible regions. For single doped PGQDs, the adsorption peaks range from 330 nm to 650 nm depending on the site and doping element. For the co-doped samples, the absorption peaks extend from the ultraviolet to the near infrared region (310 nm - 850 nm).

The obtained results have shown the influence of the doping element and the doping site on the electronic and optical properties of PGQDs. For the band narrowing of the doped structures, the transition of electrons from the valence to the conduction band of electrons is more sensitive, which in turn can increase the possible transitions, thereby increasing the number of observed spectral peaks. In addition, changes in the electronic properties of PGQD samples with impurities B, P or BP also give a peak shift to the visible region from the ultraviolet region of the pure H-36 sample. The obtained results are similar to the results of investigation of optical properties of graphene quantum dots through phosphorization or boronization in Fig. 10. The absorption peaks of graphene quantum dots through boronization appear at an energy range corresponding to 400 nm, while phosphorization produces some new absorption peaks at a longer wavelength range from 500 nm to 800 nm [19, 20]. We observe a noticeable spatial anisotropy of the optical components for PGQD-ZZ-36. There are spectral differences in the different absorption directions of these structures.

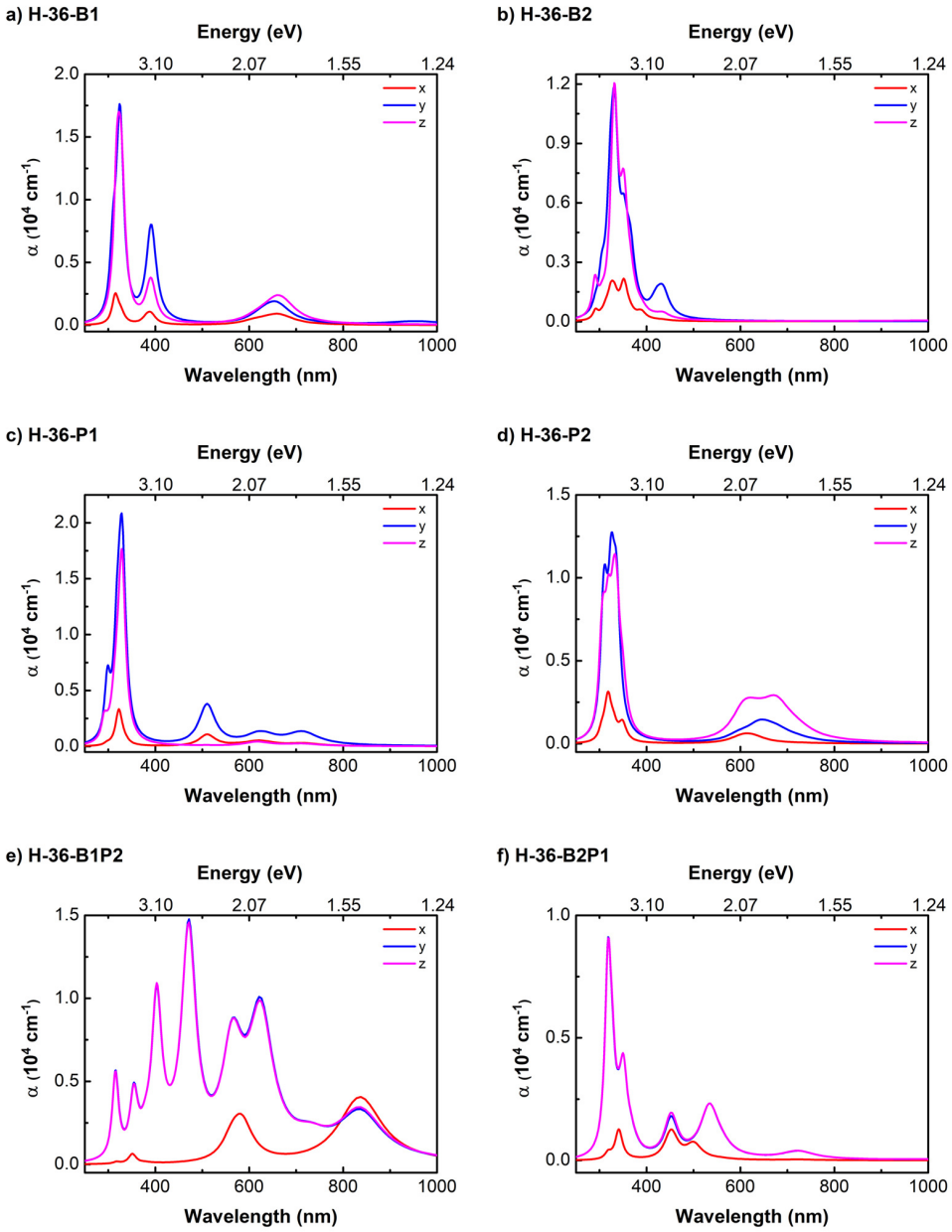

Figure 10. Optical absorption spectrum of the structures: H-36-B1, H-36-B2, H-36-P1, H-36-P2, H-36-B1P2 and H-36-B2P1.

4. Conclusion

In summary, we have successfully applied DFT calculations to systematically investigate the effect of various edge-functionalized groups (Si, P, O, and F) and doping (Si, O, B, P, or BP) on the structural stability and optoelectronic properties of penta-graphene quantum dots. The transition of electrons from the valence to the conduction band is more sensitive in Si, P, O, and F-passivated PGQDs and B, P-doped PGQDs. The changes in the electronic properties of PGQDs with impurities (Si, O, B, P, or BP) also shift the absorption spectrum toward the visible light region. The results emphasize the role of edge-functionalized groups and doping in developing the next-generation optoelectronic devices using PGQDs. Under different incident

light polarizations, the highly anisotropic morphology of edge-functionalized and doped PGQDs results in strong optical absorption anisotropy.

Acknowledgments
This work was supported by the Vietnam National Foundation for Science and Technology Development (NAFOSTED) under grant number 103.01-2020.16. This work was carried out on the Can Tho University high-computing system with the support of the Information and Network Management Center at Can Tho University.

References
[1] Lim S Y, Shen W and Gao Z, 2015 *Chem. Soc. Rev.* **44** 362.
[2] Namdari P, Negahdari B and Eatemadi A, 2017 *Biomed. Pharmacother.* **87** 209.
[3] Li X, Rui M, Song J, Shen Z and Zeng H, 2015 *Adv. Funct. Mater.* **25** 4929.
[4] Prabhu S A, Kavithayeni V, Suganthy R and Geetha K, 2021 *Carbon Lett.* **31** 1.
[5] Zhang S, Zhou J, Wang Q, Chen X, Kawazoe Y and Jena P, 2015 *Proceedings of the National Academy of Sciences* **112** 2372.
[6] Lan Y S, Chen X R, Hu C E, Cheng Y, Chen Q F, 2019 *J. Mater. Chem. A* **7** 11134.
[7] Yagmurcukardes M, Sahin H, Kang J, Torun E, Peeters F and Senger R, 2015 *J. Appl. Phys.* **118** 104303.
[8] Aierken Y, Leenaerts O, Peeters F M, 2016 *Phys. Chem. Chem. Phys.* **18** 18486.
[9] Tien N T, Thao P T B, Thuan L V P and Chuong, D H, 2022 *Comput. Mater. Sci.* **203** 111065.
[10] Liu H, Qin G, Lin Y and Hu M, 2016 *Nano letters* **16** 3831.
[11] Kuklin A V, Ågren H and Avramov P, 2020 *Phys. Chem. Chem. Phys.* **22** 8289.
[12] Dang M T, Bich Thao P T, Ngoc Thao T T and Tien N T, 2022 *AIP Adv.* **12** 065008.
[13] Deb J, Paul D and Sarkar U, 2020 *J. Phys. Chem. A*, **124** 1312.
[14] Tien N T, Thao P T B, Phuc V T and Ahuja R, 2019 *Phys. E: Low-Dimens. Syst. Nanostructures* **114** 113572.
[15] Tien N T, Thao P T B, Phuc V T and Ahuja R, 2020 *J. Phys. Chem. Solids* **146** 109528.
[16] Chen N, Wang Y, Mu Y, Fan Y and Li S D, 2017 *Phys. Chem. Chem. Phys.* **19** 25441.
[17] Li Y H, Yuan P F, Fan Z Q and Zhang Z H, 2018 *Org. Electron* **59** 306.
[18] Abdelsalam H, Elhaes H and Ibrahim M A, 2018 *Chem. Phys. Lett.* **695** 138.
[19] Feng J, Guo Q, Liu H, Chen D, Tian Z, Xia F, Ma S, Yu L and Dong L, 2019 *Carbon* **155** 491.
[20] Feng J, Dong H, Pang B, Chen Y, Yu L and Dong L, 2019 *J. Mater. Chem. C.* **7** 237.
[21] Zhang F, Liu F, Wang C, Xin X, Liu J, Guo S. Zhang J, 2016 *ACS applied materials & interfaces*, **8**(3) 2104.
[22] Elvati P. Baumeister E, Violi A, 2017 *RSC advances*, **7**(29) 17704.
[23] Clark S J, Segall M D, Pickard C J, Hasnip P J, Probert M I, Refson K and Payne M C 2005 *Cryst. Mater.* **220** 567.
[24] Perdew J P, Burke K and Ernzerhof M, 1996 *Phys. Rev. Lett.* **77** 3865.
[25] Schlipf M and Gygi F, 2015 *Comput. Phys. Commun.* **196** 36.
[26] Dal Corso A and Conte A M, 2005 *Phys. Rev. B* **71** 115106.
[27] Quinten M, 2010 *Optical properties of nanoparticle systems: Mie and beyond* (Weinheim, Germany: Wiley-VCH).
[28] Monshi M M, Aghaei S M and Calizo I, 2018 *Phys. Lett. A* **382** 1171.
[29] Li Y, Shu H, Niu X and Wang J, 2015 *J. Phys. Chem. C* **119** 24950.
[30] Dai X S, Shen T, Feng Y and Liu H C, 2019 *Phys. B: Condens. Matter* **574** 411660.